Origins of Helix−Coil Switching in a Light-Sensitive Peptide†

Darcy C. Burns,‡ Daniel G. Flint,§ Janet R. Kumita,‡ Howard J. Feldman,|| Luis Serrano,⊥ Zhihua Zhang,‡ Oliver S. Smart,§ and G. Andrew Woolley*,‡

Department of Chemistry, University of Toronto, 80 St. George Street, Toronto M5S 3H6, Canada, The Blueprint Initiative, 522 University Avenue, Toronto M5G 1W7, Canada, EMBL, Mayerhofstrasse 1, Heidelberg, D6900 Germany, and School of Biosciences, University of Birmingham, Edgbaston, Birmingham B15 2TT, United Kingdom

Received August 26, 2004; Revised Manuscript Received September 26, 2004

ABSTRACT: Intramolecular cross-linking of peptides by the light-sensitive compound diiodoacetamide-azobenzene has been shown to permit reversible photocontrol of the helix−coil transition. Cross-linking between Cys residues spaced at *i* and *i* + 7 positions with the trans form of the linker was found to produce a decreased helix content compared to that of the non-cross-linked peptide. Photoisomerization to the cis form of the linker led to substantially higher helix content than in the non-cross-linked peptide. Detailed conformational analysis of the system leads to the conclusion that photocontrol of helix content does not involve specific interactions between the linker and the peptide. Instead, the change in peptide helix content caused by photoisomerization can be predicted by comparing the length ranges of the cis and trans forms of the linker with the expected distance distribution of the Cys attachment points in the intrinsic conformational ensemble of the peptide. The analysis presented here should help to guide the use of these and related linkers for the conformational control of a variety of peptide and protein systems.

The photoisomerization of protein-bound chromophores is used by Nature to direct complex responses of biological systems to light. Examples include phototaxis in bacteria, phototropism in plants, and vision in higher organisms. Engineering-directed biochemical responses to light, if this could be accomplished in a general way, would provide an avenue for probing and manipulating complex living systems (*1*−*3*).

The azobenzene chromophore is attractive for use as a component in such engineered systems since azobenzene photoisomerization takes place quickly, with a high quantum yield, and is relatively insensitive to the local environment. In addition, azobenzene photoisomerization occurs with wavelengths of >300 nm so that the light used to produce isomerization is not strongly absorbed by the protein and nucleic acid present in biological targets (*4*−*7*).

Recently, we were successful in controlling the helix content of a JRK-X model peptide system through the incorporation of a photoisomerizable azobenzene cross-linker (*8*, *9*). A thiol-reactive azobenzene cross-linking reagent was combined with a peptide containing Cys residues spaced at positions *i* and *i* + 7 in the sequence. The dark-adapted peptide was predominantly unfolded in water and upon being exposed to light (370 nm) became substantially helical as judged by circular dichroism (CD)[1] spectroscopy. In further work, we explored *i* and *i* + 4 spacing and the *i* and *i* + 11 spacing of Cys residues. The former behaved in a manner similar to that of the *i* and *i* + 7 case, whereas the latter led to a stabilized helical conformation in the dark-adapted (trans) state and helix unfolding upon photoisomerization to the cis state (*10*, *11*).

Since α-helices are essential components of many protein structures, and since Cys residues can be introduced easily via site-directed mutagenesis, this azobenzene-based cross-linking strategy offers a general way of photocontrolling protein conformation (and thereby activity). However, to be used successfully in a rational manner, the structural basis of photocontrol of conformation must be understood. We have therefore undertaken a detailed conformational analysis of the original peptide system in an effort to understand how photoisomerization of the cross-linker causes conformational changes in the peptide.

EXPERIMENTAL PROCEDURES

Peptide Synthesis, Cross-Linking, and Purification. The peptide JRK (acetyl-EACARVAibAACEAAARQ-NH_2) was synthesized by Jerini Biotools (Berlin, Germany) using established methods. The azobenzene cross-linking reagent was synthesized and used for intramolecular cross-linking of Cys residues as detailed by Kumita and co-workers (*8*). The cross-linked form of the peptide is denoted with a terminal X following the peptide identification (i.e., JRK-X).

UV−Vis, Circular Dichroism, and Photoisomerization. UV spectra were obtained with a Perkin-Elmer Lambda 2

† This work has been supported by the Natural Sciences and Engineering Research Council of Canada (G.A.W.), the Volkswagen Stiftung, the University of Toronto (D.C.B.), and the U.K. Medical Research Council (Grant G.4600017 to O.S.S.).

* To whom correspondence should be addressed. E-mail: awoolley@chem.utoronto.ca. Phone: (416) 978-0675. Fax: (416) 978-0675.

‡ University of Toronto.

§ University of Birmingham.

|| The Blueprint Initiative.

⊥ EMBL.

[1] Abbreviations: Aib, α-aminoisobutyric acid; CD, circular dichroism; COSY, correlated spectroscopy; NOESY, nuclear Overhauser effect spectroscopy; NOE, nuclear Overhauser effect; TOCSY, total correlated spectroscopy; UV, ultraviolet.

10.1021/bi048152k CCC: $27.50
Published on Web 11/12/2004

spectrophotometer using the same thermostated quartz cell (path length of 0.1 cm) in which CD analysis was performed. Photoisomerization was accomplished by irradiating thermostated peptide solutions with a 70 W metal halide Tri-Lite lamp (World Precision Instruments) coupled to a 370 ± 10 nm band-pass filter (Harvard Apparatus Canada). Photoisomerization was complete (as judged by the lack of any further changes in UV spectra) in ≤5 min. Spectra for pure trans and cis forms of JRK-X were obtained as described previously (*9*).

Circular dichroism measurements were performed with a Jasco model J-710 spectropolarimeter. All measurements were taken in a thermostated quartz cuvette (path length of 0.1 cm). Temperatures were measured using a microprobe directly in the sample cell. All samples were dissolved in 5 mM phosphate buffer (pH 7). Reported spectra are averages of three individual experiments of five scans each, with the appropriate background spectrum subtracted. A scan speed of 10 nm/min, with a bandwidth of 0.5 nm and a response time of 4 s, was used. Using the percent cis observed by UV, theoretical 100% cis CD spectra were calculated using the equation θ(100% cis) = [θ(observed after irradiation) − fraction trans × θ(dark-adapted)]/(fraction cis).

NMR Spectroscopy of JRK-X. NMR spectra of trans-JRK-X [1.1 mM, 90% (v/v) H_2O/D_2O, pH 3.1] were obtained by placing the sample in the dark at 25 °C for a period of at least 24 h prior to acquisition. Samples containing cis-JRK-X were prepared by irradiating the NMR tube using the same 70 W metal halide Tri-Lite lamp used for CD measurements. Thermal conversion of cis-JRK-X to trans-JRK-X was minimized by immersing the NMR tube in a 100 mL graduated cylinder containing an ice/water mixture. After 45 min, the irradiated sample was returned to the magnet. The amide protons on the cross-linker provided a convenient measure of the extent of isomerization from trans- to cis-JRK-X (cis, 10.26 ppm; trans, 10.36 ppm). Under these conditions, ∼50−60% cis-JRK-X was typically obtained.

^{1}H two-dimensional (2D) TOCSY spectra of dark-adapted JRK-X and irradiated JRK-X were recorded at 800 MHz and 4 °C using the NANUC (Edmonton, AB) 800 MHz Varian Inova spectrometer equipped with a 5 mm Varian PFG probe. Some spectra were also obtained with a 500 MHz Varian Unity spectrometer equipped with a 3 mm NaloracInd3 probe. A DIPSI spin lock sequence (t_m = 60 ms) (*12*) was employed, and water suppression was achieved with a 3-9-1-9 Watergate pulse sequence (*13*). Watergate TOCSY spectra were acquired over a spectral window of 12 000 Hz (in both the f_2 and f_1 dimensions) with a gain of 26, a d_1 delay of 1 s, 512 t_1 increments, 2048 complex data points, and 16 transients. Also, 16 steady state pulses were run at the start of these experiments. Thermal relaxation of cis-JRK-X to trans-JRK-X constrained the total experiment time to 8 h so spectra were acquired with only 16 transients. Signal-to-noise ratios were maintained by acquiring and processing two identical irradiated spectra and adding these processed spectra using the madd.mac routine provided in the FELIX 2000 software package (Accelrys, San Diego, CA). Cross-peaks from trans-JRK-X and cis-JRK-X were observed in these spectra. Comparison to dark-adapted (trans) JRK-X spectra permitted assignment of cis cross-peaks.

^{1}H 2D NOESY spectra were recorded at 800 MHz and 4 °C in a fashion similar to that used for Watergate TOCSY spectra. The NOESY spectrum of trans-JRK-X was acquired (t_m = 400 ms) with 64 transients, while three spectra were acquired (16 transients; t_m = 400 ms) and processed in an additive manner for irradiated JRK-X. Other parameters for the acquisition of NOESY spectra were set as follows. Spectra were acquired over a window of 10 000 Hz (f_1) × 12 000 Hz (f_2) with a gain of 26, a d_1 delay of 1 s, 512 t_1 increments, 2048 complex data points, and 16 steady state pulses. Spectra were generally collected with a mixing time of 400 ms since studies on a closely related peptide used this condition (*14*). To determine if spin diffusion was occurring in these NOESY spectra, comparative spectra were acquired with mixing times of 200 ms. Difference restraints generated from these spectra were virtually identical to those generated with a mixing time of 400 ms.

A backbone HN chemical shift temperature dependence study was performed using the 500 MHz Varian Unity spectrometer equipped with a 3 mm NaloracInd3 probe. The Watergate TOCSY pulse sequence described above was used with the following adjustments. The spectral window was reduced to 6000 Hz (both f_1 and f_2; t_m = 80 ms), and either eight transients (dark-adapted JRK-X) or 16 transients (irradiated JRK-X) were used. Spectra were recorded at 2, 7, 12, 17, 22, and 27 °C for dark-adapted JRK-X and at 2, 7, 12, and 17 °C for irradiated JRK-X.

An 800 MHz phase-sensitive COSY spectrum of irradiated JRK-X was acquired at 4 °C for the evaluation of NH−Hα coupling constants for both trans- and cis-JRK-X. Suppression of the water signal was achieved by inserting a presaturation pulse prior to the COSY pulse sequence. COSY spectra were acquired over a spectral window of 9000 Hz (f_1) × 12 000 Hz (f_2) with a gain of 26, a d_1 delay of 1 s, 256 t_1 increments, 16K complex data points, eight steady state pulses, and 16 transients.

NMR Data Processing. Both TOCSY and NOESY spectra were analyzed using FELIX 2000 (Accelrys). The spectra were processed in the following manner. D_1 was zero-filled from 2048 complex points to 4096 points. A 60° phase-shifted sine bell squared window function was then applied to D_1, followed by Fourier transformation and appropriate phasing. Data in the D_2 dimension were linearly predicted from 512 points to 2048 points using a forward linear prediction algorithm provided by FELIX. The D_2 data set was further extended by zero-filling from 2048 points to 4096 points. A 60°-shifted sine bell squared window function was then applied to D_2, followed by Fourier transformation and appropriate phasing. These spectra were referenced on the TSP signal.

Full sequential spin system identification of trans-JRK-X and cis-JRK-X was performed according to the procedure outlined by Wüthrich (*15*) using FELIX. Eighteen spin systems were identified for both trans-JRK-X and cis-JRK-X: 16 for the main chain amino acids, another for the cross-linker, and another for the C-terminal amide moiety.

To generate distance restraints, peak volumes in the Watergate NOESY spectrum were calculated using FELIX 2000. Cross-peaks from Val6 Hβ1 to Val6 Hγ (2.70 Å) and from Cys10 Hβ1 to Cys10 Hβ2 (1.78 Å) were chosen as reference (scalar) peaks. Xplor-based NOE distance restraints were calculated for all assigned peaks. Distance restraints were categorized into small (1.5−2.5 Å), medium (1.5−3.5 Å), and weak (1.5−6.0 Å) bins.

The presat psCOSY spectrum was processed using nmrPipe (*16*). The following processing scheme was employed. The 90° phase-shifted sine bell squared window functions were applied to D_1 and D_2 prior to Fourier transformation. Data in the D_2 dimension were linearly predicted from 256 points to 512 points and then further extended by zero-filling to 4096 points. Coupling constants were determined using ACME software using the procedure described previously (*17*).

Molecular Dynamics Simulations of JRK-X. Simulated annealing (SA) molecular dynamics was used for analysis of the NOE data. The amino acid sequence of JRK (Ac-EACARVAibAACEAAARQ-NH_2) was built in SYBYL with the conformation of the peptide backbone set as random. The peptide was then subjected to energy minimization using the AMBER force field (*18*) with the PARM96 parameter set. A distance-dependent dielectric was used to implicitly represent the charge screening effects of the aqueous solvent. NOEs involving cross-linker protons were not included for analysis of the peptide backbone structure of cis-JRK-X (see the Discussion). All unique cis NOEs were included along with those involving protons of the side chains of the Glu, Arg, and Gln residues. NOEs were introduced as flat-bottomed distance restraints between hydrogen atoms. The peptide was heated to 3000 K over the course of 50 ps and then held at this temperature for a further 100 ps. The force constant for the restraints was increased from 2 to 20 kcal mol^{-1} $Å^{-2}$ after the heating stage and kept at this value for the rest of the simulation. The peptide was then slowly cooled from 3000 to 0 K over the course of 150 ps and once more subjected to energy minimization. This process was repeated 10 times, and in each case, the final structure was assessed and any deviation from the NOE distance restraints was analyzed. As a control, peptide structures were also generated by the same SA protocol without NOE restraints. The SA protocol followed for trans-JRK-X was the same except that every unambiguous NOE was included as a distance restraint for each SA run. In total, 50 runs were conducted.

For the analysis of linker dynamics, simulations of the short AACAAVAibAACA peptide (with Cys residues cross-linked by the azobenzene cross-linker) representing residues 1−11 of JRK-X were carried out. The backbone of the peptide was restrained to an α-helical conformation, and an octahedral periodic system of 1000 TIP3P waters was employed. Missing parameters describing the linker azo units were added to the AMBER force field (*19*). The system was heated from 0 to 283 K over the course of 50 ps, and then constant-pressure dynamics was performed for 200 ps to equilibrate the system to the required density. Six runs of 50 ns were then performed. For each simulation, the starting conformation of the linker was different. The first 10 ns of each simulation was discarded, and only the final 40 ns was analyzed.

Helix−Coil Modeling with SYBYL, AGADIR, and FOLDTRAJ. Conformational searches of isolated linkers with methyl groups replacing Cys β-atoms were performed using the systematic search option in SYBYL. All single bonds in the isolated linkers were rotated in 30° increments except those connecting the rings to the azo group. These, together with bond angles and bond lengths, were constrained to the values found from X-ray crystallographic studies of azobenzene (*20, 21*) and high-level computational studies (*22*).

AGADIR (http://www.embl-heidelberg.de/Services/serrano/agadir/agadir-start.html) was used to predict overall helicity as well as helix length probabilities. Normally, AGADIR calculates energies for each helix window length and from those builds the partition function to estimate overall and residue-based helicities (*23*, *24*). The program was modified simply to group calculated probabilities by helix length, sum the individual probabilities for each length, and output these. A copy of the modified program is available on request.

The "residue fragment" feature of FOLDTRAJ was used to generate an ensemble of structures with a helical content distribution matching that predicted by AGADIR. This was accomplished by adding helical fragments of various lengths to the start of the peptide, with probabilities proportional to AGADIR predictions. Effectively, this inserts ideal helical segments of varying length into an otherwise randomly generated backbone structure.

RESULTS

Photoisomerization of JRK-X

The structure of the cross-linked JRK-X peptide in cis and trans forms is shown in Figure 1A. Calorimetric measurements have found the ground state of the unmodified azobenzene chromophore to be more stable in the trans conformation than in the cis state by 49 kJ/mol (*25*). At equilibrium in the dark, unmodified azobenzene is thus only 0.0000003% cis at room temperature. Calorimetric measurements have not been performed on JRK-X; however, NMR analysis of the dark-adapted peptide reveals no trace of the cis isomer so that ≤1% would be the maximum present. Accordingly, trans-JRK-X is at least 15 kJ/mol more stable than cis-JRK-X and may be ∼50 kJ/mol more stable.

Cis-JRK-X isomerizes to trans-JRK-X in the dark via a thermal process (*5*). Rates of thermal cis-to-trans isomerization were measured for a series of temperatures by monitoring the absorbance at 370 nm after irradiation to convert a percentage of the solution to the cis isomer. The energy barrier for thermal cis-to-trans isomerization of JRK-X was calculated to be ∼78 kJ/mol.

Upon irradiation of JRK-X solutions with light at 370 ± 10 nm, excited states are produced for which the barrier to cis-to-trans isomerization is substantially smaller than the thermal barrier (Figure 1B) (*5*, *7*). Reversion to the electronic ground state after excitation thus produces a mixture of cis- and trans-JRK-X. Since cis-JRK-X does not absorb as strongly as trans-JRK-X at 370 nm (Figure 1C), irradiation of a solution of JRK-X at 370 nm produces a photostationary state that is substantially cis-JRK-X (Figure 1C). No evidence for azobenzene photobleaching was observed. The percentage of cis-JRK-X obtained depends on the relative molar extinction coefficients of the cis and trans forms at 370 nm, the quantum yield for cis-to-trans versus trans-to-cis photoisomerization, the rate of thermal reversion from cis to trans, the sample concentration, and the intensity of the light source. Using a 0.35 mW source, an ∼50 μM solution of JRK-X at 10 °C reached a photostationary state that was 77% cis as judged by an analysis of UV spectra (Figure 1B; see Experimental Procedures for details). At the concentrations required for NMR measurements, the same light source produced 50−60% cis-JRK-X.

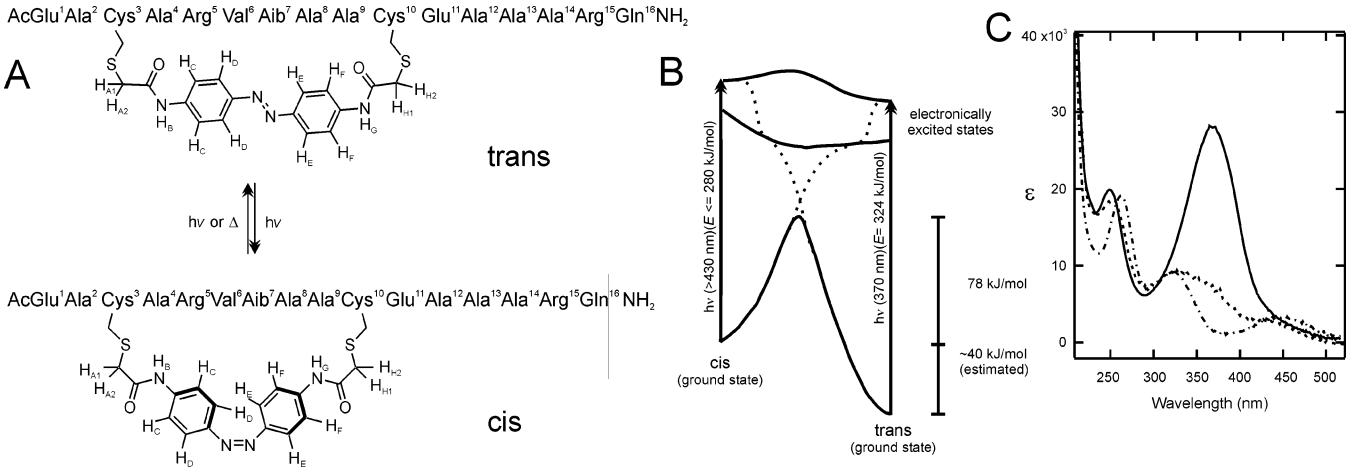

FIGURE 1: (A) Primary structure of JRK-X in trans and cis forms. (B) Simplified energy diagram for the isomerization of JRK-X. Note that the profiles of the S1 and S2 excited state surfaces are those proposed for unmodified azobenzene and are shown here for illustrative purposes only. These have not been measured in this work. (C) UV−vis spectra for trans-JRK-X (—), cis-JRK-X (-·-), and the photostationary state (···).

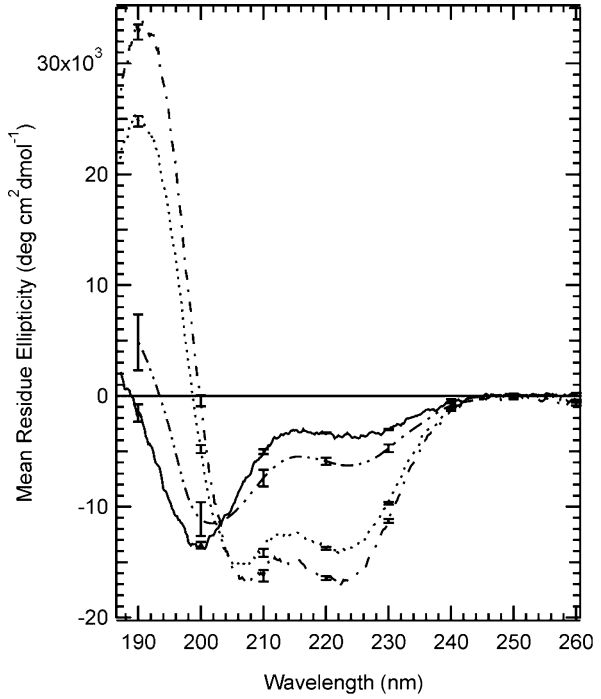

FIGURE 2: CD spectra of trans-JRK-X (—) and JRK-X upon irradiation (···) and spectrum corrected for 100% cis (-·-). The CD spectrum of non-cross-linked JRK under the same conditions is shown (-···-).

CD Analysis of Backbone Conformational Change in JRK-X

Figure 2 (solid line) shows the CD spectrum for dark-adapted JRK-X with the azobenzene moiety in the trans conformation. This spectrum is typical of a largely disordered peptide structure with a small degree of helicity (*26*). Upon irradiation with 370 nm light, the CD spectrum shown in Figure 2 (dotted line) was obtained. The intensity of the CD band at 222 nm increased; the minimum at 200 nm shifted to 207 nm, and a strong maximum at 190 nm appeared. This spectrum is characteristic of an α-helix (*26*). Under these conditions, 77% of the cis isomer is obtained on the basis of the observed UV spectrum. The CD spectrum expected for the pure cis form of the peptide can be calculated simply by correcting the 77% cis spectrum for the presence of 23% trans; the resulting spectrum is shown in Figure 2 (dashed and dotted line).

Although the CD spectrum is diagnostic for the presence of helix, a quantitative determination of helix content is complicated by the lack of consensus about the mean residue ellipticity expected for 100% helix (*27*). Using the simple assumption that 100% helix gives a θ_{222} value of $-40000 \times [(n-4)/n]$, where n is the number of residues (*28*), gives a value of 60% helix for the cis form of the peptide and 11% helix for the trans form at 10 ± 1 °C in 5 mM $NaPO_4$ (pH 7.0). For reference, the spectrum of non-cross-linked JRK is also shown (dashed and double-dotted line). This indicates a helix content for the non-cross-linked peptide of 25%, a value intermediate between those of the dark-adapted and irradiated states.

The helix−coil structural transition observed by CD upon photoisomerization was fully reversible. CD spectra of varying percentages of cis-JRK-X exhibited an isodichroic point at 203 nm which suggests the existence of a simple two-state equilibrium between helical and disordered forms of the peptides (*29*). CD spectra were independent of peptide concentration over a range of 5−225 μM, indicating the absence of self-association. Similarly, no evidence for self-association was observed in NMR samples with a concentration of >2 mM.

NMR Analysis of the Backbone Conformational Change in JRK-X

^{1}H NMR spectra were recorded for dark-adapted JRK-X and irradiated JRK-X in a 90% H_2O/10% D_2O mixture at pH 3.1 and 4 °C, conditions similar to those used for the CD measurements. The lower pH was used to decrease amide exchange rates and optimize the resolution of NH chemical shifts. A lowered pH caused only a slight decrease in helicity of cis-JRK-X as judged by the intensity of the CD signal at 222 nm and had no effect on the CD of trans-JRK-X. The half-life of cis-JRK-X is ~4 h at this temperature and pH. Standard TOCSY, COSY, and NOESY spectra were acquired using established methods (*14*). Sixteen spin systems were identified for trans-JRK-X by analysis of dark-adapted spectra. A further 16 spin systems for cis-JRK-X were identified in irradiated spectra. There was no evidence for

multiple conformations exchanging slowly on the NMR time scale as has been reported for some other azobenzene-containing cyclic peptides (*30*). Spin system connectivities were determined from the NH−NH region of the ^{1}H−^{1}H NOESY spectra. In addition to the amino acid spin systems, trans- and cis-JRK-X linker chemical shifts were identified (Tables I and II of the Supporting Information).

Chemical Shift Analysis. NMR chemical shifts are useful qualitative markers of structural elements in peptides (*31*). Residues in helices typically show Hα chemical shifts upfield of their random coil values. Residues in β-strand extended conformations show a comparable downfield shift. For trans-JRK-X, five of 15 Hα resonances are shifted upfield of their respective random coil values. Cis-JRK-X has 12 of 15 Hα chemical shifts upfield of their random coil values (Aib7 does not have an α-proton). No shifts downfield of random coil values were observed.

Chemical Shift Temperature Gradients. Andersen et al. (*32*) have presented a detailed analysis of the relationship between the temperature dependence of peptide NH backbone chemical shifts and peptide conformation. In the absence of temperature-induced conformational changes, amide proton chemical shifts exhibit a temperature dependence that is influenced by their hydrogen bonding environment (*33*). Intramolecularly hydrogen-bonded NHs typically show $\Delta\delta/\Delta T$ values of -2 ± 1.4 ppb/°C, while solvent-exposed NHs typically display gradients between −5 and −11 ppb/°C (*32*). Trans-JRK-X NHs exhibited $\Delta\delta/\Delta T$ values more negative than −5 ppb/°C for 13 of 15 residues. In contrast, 13 of 16 cis-JRK-X NH shifts have $\Delta\delta/\Delta T$ values more positive than −4 ppb/°C.

Peptide conformational changes with temperature (e.g., helix unfolding) will also contribute to the observed chemical shift temperature gradients, and may dominate them (*32*). For flexible peptide systems, Andersen et al. have proposed using correlations between NH chemical shift temperature gradients and NH chemical shift deviations from random coil values as indicators of changes in conformational equilibria (*32*). Using their approach, we find a correlation coefficient (R) of 0.3 and a slope of −1.2 ppt/°C for trans-JRK-X. These values increase to 0.6 and −7.3 ppt/°C, respectively, for cis-JRK-X, indicating a shift toward a dominant helical conformational state with a mole fraction on the order of 0.35−0.7 (*32*). Positive NH temperature coefficients observed for Arg15 and Gln16 in cis-JRK-X may reflect fraying at the C-terminal end of a helical structure.

Coupling Constants (NH−Hα). Scalar coupling constants between NH and Hα protons are sensitive to backbone ϕ (φ) angles (*15*, *34*). $^3J_{HN\alpha}$ values of ≤4 Hz are typical of helical conformations, whereas extended conformations typically give coupling constants of >9 Hz (*31*, *34*). Figure 3A shows the NH−Hα region of a ^{1}H−^{1}H COSY spectrum of an irradiated sample of JRK-X. Trans-JRK-X peaks are colored blue, and cis-JRK-X peaks are colored red. Coupling constants were extracted from this spectrum using ACME (*17*) and are compiled in Figure 3B. Trans-JRK-X coupling constants are consistent with extensive averaging of conformations, whereas cis-JRK-X coupling constants are generally less than 5 Hz with several less than 4 Hz, consistent with a significant fraction of helical structure. The larger coupling constants of Arg15 and Gln16 are consistent with some C-terminal fraying of the helix.

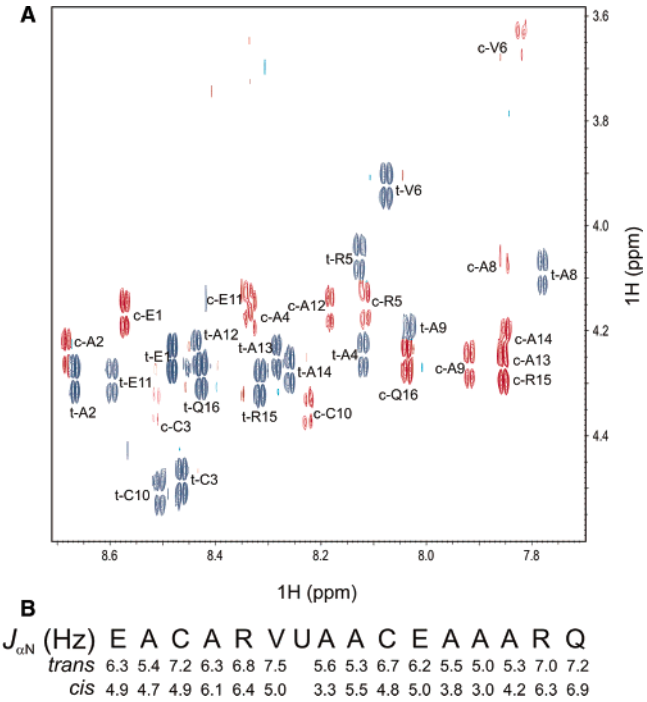

FIGURE 3: (A) ^{1}H−^{1}H COSY spectrum of JRK-X. Trans cross-peaks are blue, and cis cross-peaks are red. (B) Measured coupling constants between NH and Hα protons.

Nuclear Overhauser Effects. NOE measurements are useful indicators of secondary structure even in peptide systems that are expected to adopt multiple conformations in solution (*14*). Medium-range NOEs of the NH−NH (i, i + 1) type are considered indicative of helical structure (*35*). Only one such NOE was observed for trans-JRK1-X, where Aib is at position i. This is probably because the ϕ and ψ angles of Aib are restricted to helical space (*36*), and thus, there is local helicity at this residue. The lack of NH−NH (i, i + 1) NOEs implies the trans peptide is, overall, not helical. Indeed, analysis of the complete set of trans-JRK-X NOEs gave no pattern indicative of conformational preferences of the peptide backbone, the peptide side chains, or the cross-linker. Using the observed NOEs as distance restraints, trans-JRK-X structures were produced using the simulated annealing protocol described in Experimental Procedures. No overall secondary structural preference was noted. A cluster analysis was performed using Moil-View (*37*) in which all the structures were overlaid by fitting the heavy atoms of the cross-linker. The peptide backbones of the 50 structures were not observed to preferentially occupy any region of space around the cross-linker.

In contrast, NOESY spectra of cis-JRK-X provided several strong indicators for the presence of substantial helical structure. For instance, three Hα−HN (i, i + 3) NOEs (between residues 3 and 6, 6 and 9, and 8 and 11) were observed, all of which are intermediate in intensity, indicating the presence of conformations in which these protons are <4 Å apart.

When Val and Aib occur consecutively in a peptide, the relative locations of the four methyl groups (two α-methyl groups of Aib and two γ-methyl groups of Val) provide excellent indicators of local α-helicity. All the NOEs observed between Val6 and Aib7 for cis-JRK-X together with predicted distances between protons in these two residues when the peptide backbone adopts an α-helical conformation

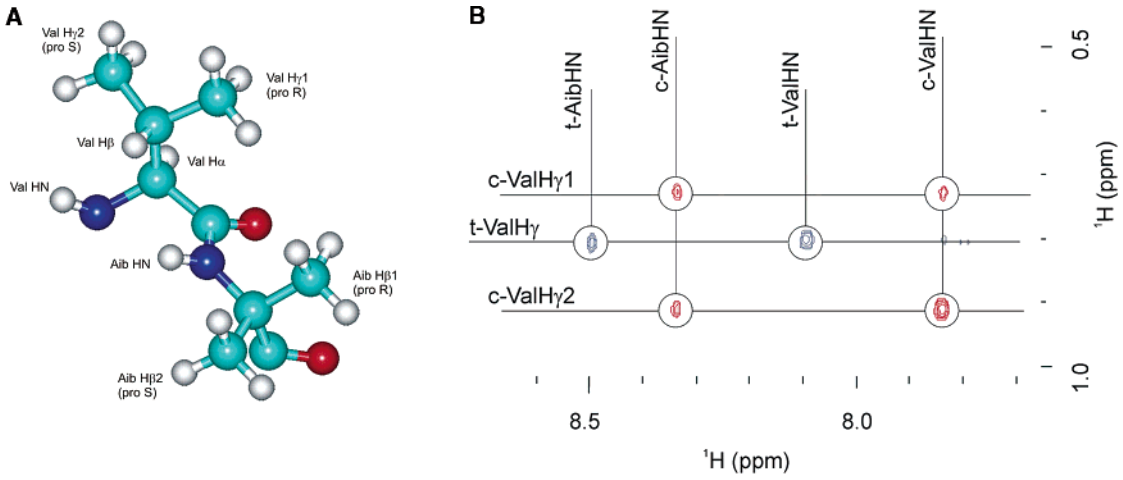

C

		VAL								AIB					
		Hα		Hβ		Hγ1		Hγ2		HN		Hβ1		Hβ2	
		NOE	Distance in helix/ Angstrom	NOE	Distance in helix/ Angstrom	NOE	Distance in helix/ Angstrom	NOE	Distance in helix/ Angstrom	NOE	Distance in helix/ Angstrom	NOE	Distance in helix/ Angstrom	NOE	Distance in helix/ Angstrom
VAL	HN	I	2.9	I	2.4	I	4.1	I	3.0	W	2.9	x	5.8	I	5.2
	Hα	-	-	I	3.0	I	2.9	S	2.6	I	3.6	x	5.2	x	5.7
	Hβ	-	-	-	-	S	2.1	S	2.2	I	2.7	x	4.8	x	5.1
	Hγ1	-	-	-	-	-	-	I	2.5	I	3.8	I	4.5	W	5.7
	Hγ2	-	-	-	-	-	-	-	-	I	4.5	x	6.4	x	6.9
AIB	HN	-	-	-	-	-	-	-	-	-	-	I	3.1	W	2.5
	Hβ1	-	-	-	-	-	-	-	-	-	-	-	-	S	2.4

FIGURE 4: (A) Ball-and-stick representation of Val and Aib as part of an α-helix. Atom coloring is as follows: cyan for C, white for H, red for O, and blue for N. (B) Section of the ^{1}H−^{1}H NOESY spectrum showing Val γCH3 cross-peaks to Val and Aib NH protons. In cis-JRK-X, the *pro-R* and *pro-S* γ-methyl groups of Val6 have substantially different chemical shifts, whereas in the trans form of the peptide, they have overlapping chemical shifts. (C) Observed NOEs between individual protons or methyl proton groups are listed along with the distance in angstroms of these protons in an AMBER-minimized α-helix. Distances involving methyl hydrogens are measured from the center of the carbon atom. NOE strengths are represented by a single-letter code: S for strong, I for intermediate, W for weak, and x for no NOE observed.

are shown in Figure 4. These NOE data are only consistent with the peptide backbone of both residues adopting an α-helical conformation.

In an α-helix, a carbon or sulfur γ-atom is sterically hindered from adopting a gauche$^-$ (60°) χ_1 conformation. Thus, for a β-branched residue such as valine, only the β-hydrogen is sterically allowed to occupy this position (*38*). The presence of substantial helical structure would thus restrict the range of chemical environments sensed by the γ-methyl protons of Val6. Consistent with this is the observation that for cis-JRK-X the *pro-R* and *pro-S* γ-methyl groups of Val6 have substantially different chemical shifts, whereas in the trans form of the peptide, they have overlapping chemical shifts. Likewise, the *pro-R* and *pro-S* methyl groups of Aib have different chemical shifts in cis-JRK-X and overlapping shifts in trans-JRK-X (Figure 3, Tables I and II of the Supporting Information). The presence of a helical secondary structure has previously been reported to cause differential shifts for *pro-R* and *pro-S* methyl groups of Aib (*39*).

In each of the energy-minimized structures produced following simulated annealing, the peptide backbone of residues 1−12 adopted a continuous α-helix. Peptide structures generated by the same simulated annealing protocol but without NOE restraints adopted only disordered conformations. However, even with all the NOE distance restraints included, the backbone of residues 13−16 adopted no consistent conformation. The side chains of Arg5, Arg15, Glu11, and Gln16 also showed no consistent conformational preferences, indicating that each likely populates several different conformers with no single conformer being significantly preferred.

Conformational Behavior of the Azobenzene Cross-Linker

For both cis and trans forms of the cross-linker, a single set of resonances were observed, indicating a single conformation or, more likely, a rapidly averaging set of conformations. Moreover, protons on the aromatic rings that interconvert through ring rotation [e.g., H_C (Figure 1)] were equivalent at 800 MHz, indicating rapid rotation of the chromophore on the NMR time scale. This result indicates that no strong, noncovalent interactions occur between the cross-linker and the peptide in either trans or cis conformations. Since the peptide backbone of trans-JRK-X appears to have no significant conformational preferences, a mobile cross-linker in trans-JRK-X is not surprising. NOEs between the cross-linker and the peptide were included in simulated annealing of trans-JRK-X and led to no consistent conformational pattern.

In the case of cis-JRK-X, rotation about the $N_{azo}-C_{aromatic}$ bonds in the cis azobenzene moiety will lead to changes in the twist sense (Δ vs Λ) of the cross-linker. The observation of a single shift for H_C (Figure 1, Table II of the Supporting Information) indicates that these isomers interconvert quickly.

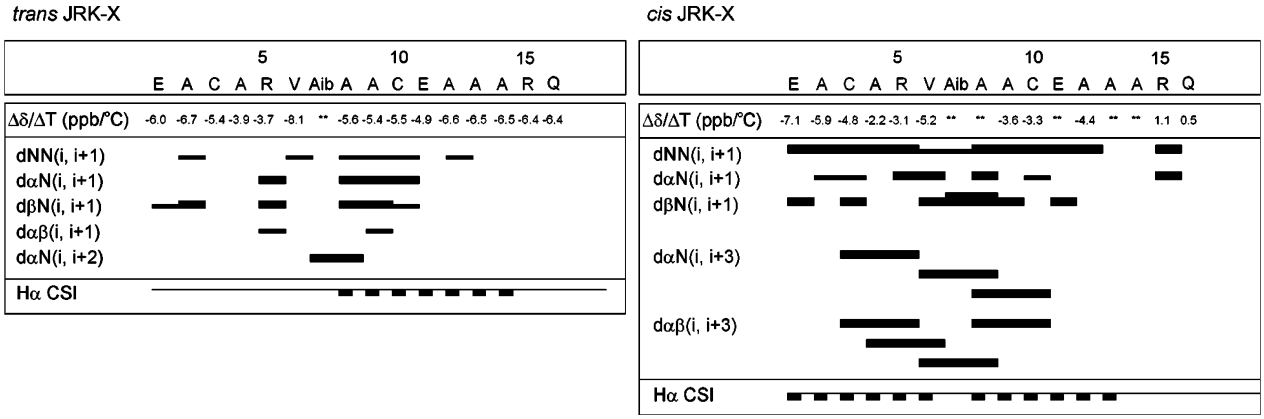

FIGURE 5: Summary of conformational parameters derived from NMR data.

That the conformation of the cis linker is dynamic is also supported by the NOE data. Nine NOEs were observed between the aromatic and amide linker protons and the methyl protons of Val and Aib side chains of the cis-JRK-X peptide. Of these, five were between the linker and Val and four between the linker and Aib. Because of the distances between these amino acid side chains in an α-helix, the linker must move between at least two conformations (one in which it is near the Val side chain and one near the Aib methyl groups) to satisfy the distance requirements for producing all these NOEs.

DISCUSSION

Two central questions were addressed in this study. (i) What is the detailed nature of the light-induced conformational change in the JRK-X peptide? (ii) What is the mechanism whereby cis-to-trans isomerization of the chromophore induces this change?

What Is the Detailed Nature of the Light-Induced Conformational Change in the JRK-X Peptide? A detailed analysis of the $^1H-^1H$ COSY and $^1H-^1H$ NOESY spectra was carried out to extract information about the conformations of the trans and cis forms of JRK-X. A summary of peptide backbone conformational data extracted from the NMR analyses of cis and trans-JRK-X is presented in Figure 5. For trans-JRK-X, chemical shift data, NH/Hα chemical shift temperature dependences, NH/Hα coupling constants, and NOE data all point to a family of disordered conformations with extensive conformational averaging and NH−solvent H-bonding. CD data are also consistent with this conclusion.

For the cis peptide, chemical shift data, NH−Hα chemical shift temperature dependences, and NH−Hα coupling constants and NOE data all point to substantial helical content at least residues 2−11. There is no NOE evidence for or against helicity for residues 12−16, but chemical shift data, NH−Hα chemical shift temperature dependences, and NH−Hα coupling constants all support helicity at the C-terminal end of the peptide. There is no evidence for dominant conformations of the side chains of Arg5, Glu11, Arg15, or Gln16. It is expected that these are generally mobile and surrounded by solvent. The peptide thus displays considerable helix content but at the same time is likely sampling a variety of unfolded conformations. These lead to averaging of side chain Val dihedral angles, for instance, as well as some averaging of backbone dihedrals. Indeed, it would be highly unlikely that a peptide of this size would adopt a single conformation in water. Fraying from the C-terminal end is also not unexpected (*40*).

The cross-linker itself appears to be mobile in both cis and trans conformations on the basis of the absence of any NMR peaks that could be attributed to restricted rotation of either of the azobenzene rings. For the cis form, NOE cross-peaks suggested that the linker adopted at least two preferred families of conformations: one in which it was close to the Val side chain and the other in which it was close to Aib. This hypothesis was tested with molecular dynamics (MD) simulations. A total of 240 ns of simulation was performed on a fully solvated but simplified cis-JRK-X peptide in which Arg and Glu side chains were changed to Ala. A helical structure was maintained by adding backbone constraints. As hypothesized, two main conformational populations were found in which the linker was either interacting with the Val side chain or the Aib methyl groups (Figure 6).

At no point during any of the simulations was the linker near both the Val and Aib residues at the same time. The relative populations for each state were averaged over all simulations (Figure 6). Both the near-Val and near-Aib positions of the linker were fairly stable on the time scale of the MD simulations. During the total simulation time of 240 ns, a change from one state to the other was only observed 11 times. Interconversion between the Δ and Λ forms was monitored by recording the value of the C−C−N═N bond torsion angles for each ring (Figure 6). Numerous interconversions between the Δ and Λ forms were observed during the simulations. A preference for the Δ form (right-handed) was observed when the linker was close to either the Val or Aib residue, but not when is was near neither residue.

What Is the Mechanism whereby Cis-to-Trans Isomerization of the Chromophore Induces This Conformational Change? Since the linker is mobile, backbone conformational change does not seem to be driven by high-affinity, noncovalent stabilizing interactions between the linker and the peptide, for instance, between the cis form of the linker and the underlying residues. This conclusion is supported by the finding that varying these amino acids does not appear to have a substantial effect on the conformational transition (e.g., Ala, Ala in place of Val, Aib) (*9*). This leaves instead steric effects caused by the change in linker length upon isomerization as the likely cause of the conformational change.

(A)

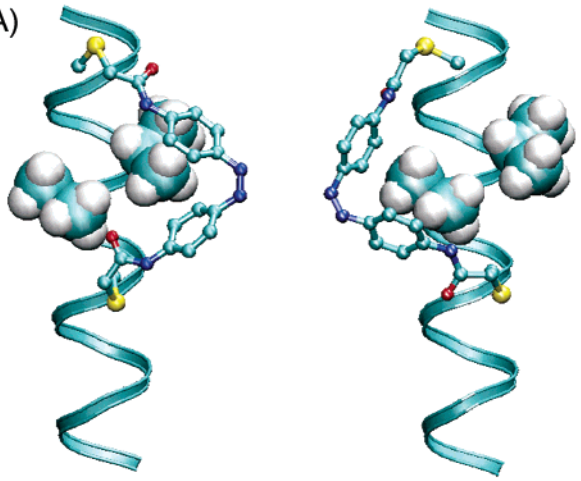

(B)

Position of the linker	near Val (C_{azo1} to $C_{\gamma 2}$ < 8Å)*	near Aib (C_{azo1} to Cβ2 < 8Å)	near neither (C_{azo1} to Cβ2 > 8Å and C_{azo1} to $C_{\gamma 2}$ > 8Å)
Percentage	49.4	43.0	7.6

* C_{azo1} refers to the carbon next to the azo nitrogen in the phenyl nearest the N-terminus of the peptide.

	approx. C-C-N=N ring1 (N-term)	approx. C-C-N=N ring2 (C-term)	near Val	near Aib	near neither
Right handed (P or Δ)*	45	-135	77.0	82.5	58.5
Left Handed	-45	135	23.0	17.5	41.5

*The sign of the smaller torsion angle between the fiducial groups defines the chirality sense of the azobenzene unit.

FIGURE 6: (A) Two conformations of the linker observed during MD simulation of cis-JRK-X. The azobenzene rings are near the Val residue in the image on the left and near the Aib residue in the image on the right. Peptide backbones are represented as ribbons; the side chains of Val and Aib are shown as space-filling diagrams, and the linker is in stick format. (B) Summary of linker dynamics from MD simulations of cis-JRK-X.

Previous studies on the effects of intramolecular cross-links on helix−coil transitions, and on protein folding in general, have been treated by considering the reduction in entropy of the unfolded state induced by the linker (*41*−*43*). For the helix−coil transition in particular, cross-links are often described in terms of increasing the probability of nucleation (σ in Zimm−Bragg or v^2 in Lifson−Roig helix−coil transition theory). A detailed study by Kise and Bowler (*41*) on the effect of a Ru(III)-induced cross-link between His residues showed, however, that both nucleation and propagation parameters were affected.

A similar approach to the one employed by Kise and Bowler might be employed here to assess the effects of the azobenzene cross-linker on the JRK-X helix−coil transition. However, while the cis form is expected to decrease the entropy of the coil state and be compatible with a helical conformation, the trans form of the cross-linker decreases both the entropy of the coil state *and* the stability of the helical state. Moreover, the description of the effects of the cross-linker in terms of modified initiation and propagation parameters does not easily lead to an understanding of what aspects of the linker (e.g., length and flexibility) are important for inducing the observed transition. Such an understanding would help in the rational application of the cross-linker as well as in the design of improved cross-linkers.

Therefore, in an effort to understand, in a quantitative manner, the observed change in helix content, we began by considering what the distribution of Cys−Cys distances would be in the non-cross-linked peptide. This distance is not directly available experimentally from the NMR data, and molecular dynamics simulations may not reliably provide an equilibrium distribution of the distance. However, standard helix−coil transition theory successfully describes the equilibrium conformational behavior of short monomeric peptides in water (*44*). In particular, the AGADIR formalism and algorithm shows excellent predictive ability (*23*, *24*). When the sequence of the non-cross-linked JRK peptide (with Ala substituting for Aib since AGADIR is not parametrized for Aib) is provided as input, together with solution conditions from the CD measurements (10 °C, 10 mM phosphate buffer, and pH 7), AGADIR predicts a helix content of 21%, a value in good agreement with the helix content of 25% estimated above. Indeed, the Aib for Ala substitution would be likely to increase the helix content slightly (*36*). A modification to the AGADIR program was then made so that, in addition to predicting overall helix content, helix length probabilities were also calculated (i.e., the probability of a helix of length x occurring anywhere in the 16-residue peptide, where x varies from 4 to 16).

The helix content and distributions predicted by AGADIR were then used as input for FOLDTRAJ. FOLDTRAJ is a probabilistic all-atom protein structure sampling algorithm (*45*). It uses geometrical constraints together with a Lennard-Jones type potential for self-avoidance and is capable of rapidly sampling conformational space without lattices. We used FOLDTRAJ to generate a family of ∼100000 structures of non-cross-linked JRK. The overall helix content in this distribution and the distribution of helix lengths matched closely that predicted by AGADIR. The structures generated by FOLDTRAJ were then used to produce a probability distribution of distances between Cys sulfur atoms for the conformational ensemble. This distribution is shown in Figure 7.

Despite the relatively low overall helix content, the distribution is sharply peaked at the Cys−Cys (S−S) distance expected for a standard α-helical conformation (∼10.8 Å). Similar peaked distributions for peptide end-to-end distances have been reported previously as part of a Monte Carlo statistical mechanical study of the helix−coil transition using a hard-sphere model of polyalanine based on Lifson−Roig theory (*46*). Note that JRK peptides with very low total helix content (∼5%) show a broad distribution with a maximum at longer S−S distances (Figure 7, dotted line).

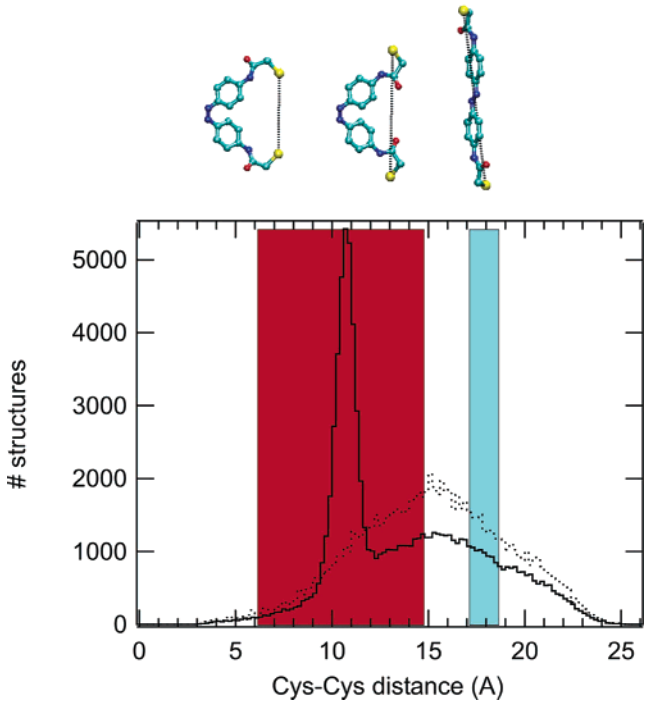

FIGURE 7: Histogram showing the distribution of Cys−Cys (S−S) distances (0.2 Å intervals) expected for the non-cross-linked JRK peptide under the conditions of the CD experiments (overall helix content of 27%) (—). The dotted line shows the expected distribution for non-cross-linked JRK where the overall helix content is 5% (e.g., at high temperatures). The total number of structures was 90 266 in each case. The distance range allowed by a cis cross-linker is shaded red; that allowed by a trans cross-linker is shaded cyan. Some representative linker structures are shown above. The bent forms of the cross-linker result in a greater range of S−S distances as single bonds rotate.

Covalent attachment of an azobenzene cross-linker must constrain this distribution. To a first approximation, let us suppose the constraints are primarily steric; that is, the linker simply does not allow S−S distances outside a particular range, the allowed ranges being different for cis and trans conformations of the linker. To estimate what these ranges are, we performed systematic conformational searches of each isomer of the linker by rotating each single bond in the structure as described in Experimental Procedures. The range of S−S distances was found to be 6−14.6 Å for the cis form (red area in Figure 7) and 17.1−18.7 Å for the trans form (blue area in Figure 7).

The range of distances available to the cis form is larger than the range available to the trans form as a consequence of the bent structure. Note that we have not made any attempt to rank the relative energies of these forms; the intent was simply to examine the range of S−S distances that would be available to the isolated cross-linkers. When these ranges are superimposed upon the distribution of S−S distances for the non-cross-linked JRK peptide (Figure 7), it is immediately evident that the cis range encompasses the spike in the distribution at 10.8 Å whereas the trans range does not. If one then calculates the helix content associated with each of these subsets of peptide structures (available from the FOLDTRAJ output), one finds 48% helix for the cis range and 2% helix for the trans range. This result is a direct consequence of the greater likelihood of a long helix occurring near the 10.8 Å peak.

This simple analysis thus describes semiquantitatively the nature of the observed effect; i.e., trans-to-cis isomerization of the covalently attached linker causes a very substantial increase in helix content (2% predicted vs 11% experimental for the trans conformation; 47% predicted vs 60% experimental for the cis form) simply by restricting S−S distance ranges. There are a variety of possible reasons for the inexactness of these predictions. First, the ranges of S−S distances calculated are only approximate and do not take into account the bond and torsion angles required to make the covalent attachment of the peptide to the linker. In addition, no account is taken of possible steric clashes between the linker and the peptide.

The analysis presented here, while simplified, does provide a straightforward means for thinking about how linker structure affects the peptide conformational transition. For instance, it suggests that if the conformation of the cis linker were more restrictive, so that only distances between 10 and 12 Å were permitted, even greater helix content for the cis cross-linked peptide might result. However, it may be that as the switch (or the peptide) becomes more conformationally demanding the dynamics and the energetics of isomerization are affected. The analysis also implies that for peptides with near-zero helix content, i.e., pure random coil, cis-to-trans isomerization of an attached linker would have little effect on helix content since the helix content of both cis-allowed and trans-allowed S−S ranges would be low. Consistent with this prediction, the difference in helix content between cis and trans cross-linked JRK peptides is observed to decrease with an increase in temperature (*8*).

In summary, we have shown that the effect of cross-linker photoisomerization on the equilibrium helix content of an attached peptide can be predicted by comparing the range of S−S distances in the intrinsic conformational ensemble of the peptide with the range compatible with the chemical structure of the linker. This analysis provides a framework for the rational application of this and related intramolecular cross-linkers to the control of peptide and protein structure.

ACKNOWLEDGMENT

NMR spectra were acquired at NANUC. Modeling support was provided by the Molecular Design and Information Technology (MDIT) Center (Toronto, ON).

SUPPORTING INFORMATION AVAILABLE

Residue and linker assignments for cis- and trans-JRK-X. This material is available free of charge via the Internet at http://pubs.acs.org.

REFERENCES

1. Liang, X., Asanuma, H., Kashida, H., Takasu, A., Sakamoto, T., Kawai, G., and Komiyama, M. (2003) NMR study on the photoresponsive DNA tethering an azobenzene. Assignment of the absolute configuration of two diastereomers and structure determination of their duplexes in the trans-form, *J. Am. Chem. Soc. 125*, 16408−16415.
2. Shimizu-Sato, S., Huq, E., Tepperman, J. M., and Quail, P. H. (2002) A light-switchable gene promoter system, *Nat. Biotechnol. 20*, 1041−1044.
3. Schutt, M., Krupka, S. S., Milbradt, A. G., Deindl, S., Sinner, E. K., Oesterhelt, D., Renner, C., and Moroder, L. (2003) Photocontrol of cell adhesion processes: model studies with cyclic azobenzene-RGD peptides, *Chem. Biol. 10*, 487−490.

4. James, D. A., Burns, D. C., and Woolley, G. A. (2001) Kinetic characterization of ribonuclease S mutants containing photoisomerizable phenylazophenylalanine residues, *Protein Eng. 14*, 983−991.
5. Rau, H. (1990) in *Photochromism. Molecules and Systems* (Durr, H., and Bouas-Laurent, H., Eds.) pp 165−192, Elsevier, Amsterdam.
6. Bredenbeck, J., Helbing, J., Sieg, A., Schrader, T., Zinth, W., Renner, C., Behrendt, R., Moroder, L., Wachtveitl, J., and Hamm, P. (2003) Picosecond conformational transition and equilibration of a cyclic peptide, *Proc. Natl. Acad. Sci. U.S.A. 100*, 6452−6457.
7. Sporlein, S., Carstens, H., Satzger, H., Renner, C., Behrendt, R., Moroder, L., Tavan, P., Zinth, W., and Wachtveitl, J. (2002) Ultrafast spectroscopy reveals subnanosecond peptide conformational dynamics and validates molecular dynamics simulation, *Proc. Natl. Acad. Sci. U.S.A. 99*, 7998−8002.
8. Kumita, J. R., Smart, O. S., and Woolley, G. A. (2000) Photocontrol of helix content in a short peptide, *Proc. Natl. Acad. Sci. U.S.A. 97*, 3803−3808.
9. Kumita, J. R., Flint, D. G., Smart, O. S., and Woolley, G. A. (2002) Photo-control of peptide helix content by an azobenzene cross-linker: steric interactions with underlying residues are not critical, *Protein Eng. 15*, 561−569.
10. Flint, D. G., Kumita, J. R., Smart, O. S., and Woolley, G. A. (2002) Using an azobenzene cross-linker to either increase or decrease peptide helix content upon trans-to-cis photoisomerization, *Chem. Biol. 9*, 391−397.
11. Chen, E., Kumita, J. R., Woolley, G. A., and Kliger, D. S. (2003) The kinetics of helix unfolding of an azobenzene cross-linked peptide probed by nanosecond time-resolved optical rotatory dispersion, *J. Am. Chem. Soc. 125*, 12443−12449.
12. Shaka, A., Lee, C., and Pines, A. (1988) Iterative schemes for bilinear operations: Application to spin decoupling, *J. Magn. Reson. 77*, 274−293.
13. Piotto, M., Saudek, V., and Sklenar, V. (1992) Gradient-tailored excitation for single-quantum NMR spectroscopy of aqueous solutions, *J. Biomol. NMR 2*, 661−665.
14. Merutka, G., Morikis, D., Bruschweiler, R., and Wright, P. E. (1993) NMR evidence for multiple conformations in a highly helical model peptide, *Biochemistry 32*, 13089−13097.
15. Wuthrich, K. (1986) *NMR of Proteins and Nucleic Acids*, John Wiley & Sons, New York.
16. Delaglio, F., Grzesiek, S., Vuister, G. W., Zhu, G., Pfeifer, J., and Bax, A. (1995) NMRPipe: a multidimensional spectral processing system based on UNIX pipes, *J. Biomol. NMR 6*, 277−293.
17. Delaglio, F., Wu, Z., and Bax, A. (2001) Measurement of homonuclear proton couplings from regular 2D COSY spectra, *J. Magn. Reson. 149*, 276−281.
18. Cornell, W. D., Cieplak, P., Bayly, C. I., Gould, I. R., Merz, K. M., Ferguson, D. M., Spellmeyer, D. C., Fox, T., Caldwell, J. W., and Kollman, P. A. (1995) A second generation force field for the simulation of proteins, nucleic acids, and organic molecules, *J. Am. Chem. Soc. 117*, 5179−5197.
19. Flint, D. G. (2003) in *School of Biosciences*, pp 219, University of Birmingham, Birmingham, U.K.
20. Robertson, J. M. (1939) Crystal Structure and Configuration of the Isomeric Azobenzenes, *J. Chem. Soc.*, 232−236.
21. Brown, C. J. (1966) A refinement of the crystal structure of azobenzene, *Acta Crystallogr. 21*, 146−152.
22. Fliegl, H., Kohn, A., Hattig, C., and Ahlrichs, R. (2003) Ab initio calculation of the vibrational and electronic spectra of trans- and cis-azobenzene, *J. Am. Chem. Soc. 125*, 9821−9827.
23. Munoz, V., and Serrano, L. (1994) Elucidating the folding problem of helical peptides using empirical parameters, *Nat. Struct. Biol. 1*, 399−409.
24. Munoz, V., and Serrano, L. (1997) Development of the multiple sequence approximation within the AGADIR model of α-helix formation: comparison with Zimm-Bragg and Lifson-Roig formalisms, *Biopolymers 41*, 495−509.
25. Dias, A. R., Minas da Piedade, M. E., Martinho Simoes, J. A., Simoni, J. A., Teixeira, C., Diogo, H. P., Meng-Yan, Y., and Pilcher, G. (1992) Enthalpies of formation of cis-azobenzene and trans-azobenzene, *J. Chem. Thermodyn. 24*, 439−447.
26. Johnson, W. C., Jr. (1990) Protein secondary structure and circular dichroism: a practical guide, *Proteins 7*, 205−214.
27. Chin, D. H., Woody, R. W., Rohl, C. A., and Baldwin, R. L. (2002) Circular dichroism spectra of short, fixed-nucleus alanine helices, *Proc. Natl. Acad. Sci. U.S.A. 99*, 15416−15421.
28. Kallenbach, N. R., and Spek, E. J. (1998) Modified amino acids as probes of helix stability, *Methods Enzymol. 295*, 26−41.
29. Rohl, C. A., and Baldwin, R. L. (1998) Deciphering rules of helix stability in peptides, *Methods Enzymol. 295*, 1−26.
30. Renner, C., Behrendt, R., Sporlein, S., Wachtveitl, J., and Moroder, L. (2000) Photomodulation of conformational states. I. Mono- and bicyclic peptides with (4-amino)phenylazobenzoic acid as backbone constituent, *Biopolymers 54*, 489−500.
31. Case, D. A., Dyson, H. J., and Wright, P. E. (1994) Use of chemical shifts and coupling constants in nuclear magnetic resonance structural studies on peptides and proteins, *Methods Enzymol. 239*, 392−416.
32. Andersen, N. H., Neidigh, J. W., Harris, S. M., Lee, G. M., Liu, Z., and Tong, H. (1997) Extracting information from the temperature gradients of polypeptide NH chemical shifts. 1. The importance of conformational averaging, *J. Am. Chem. Soc. 119*, 8547−8561.
33. Llinas, M., and Klein, M. (1975) Solution conformation of ferrichromes. 6. Charge-relay at peptide-bond−proton magentic resonance study of solvation effects on amide electron density distribution, *J. Am. Chem. Soc. 97*, 4731−4737.
34. Bystrov, V. F. (1976) Spin−spin coupling and the conformational states of peptide systems, *Prog. NMR Spectrosc. 10*, 41−81.
35. Billeter, M., Braun, W., and Wuthrich, K. (1982) Sequential resonance assignments in protein ^{1}H nuclear magnetic resonance spectra. Computation of sterically allowed proton−proton distances and statistical analysis of proton−proton distances in single-crystal protein conformations, *J. Mol. Biol. 155*, 321−346.
36. O'Neil, K. T., and DeGrado, W. F. (1990) A thermodynamic scale for the helix-forming tendencies of the commonly occurring amino acids, *Science 250*, 646−651 [published erratum, (1991) *Science 253* (5023), 952].
37. Simmerling, C., Elber, R., and Zhang, J. (1995) in *Modelling of Biomolecular Structure and Mechanisms* (Pullman, A., Ed.) pp 241−265, Kluwer, Amsterdam.
38. Yun, R. H., and Hermans, J. (1991) Conformational equilibria of valine studied by dynamics simulation, *Protein Eng. 4*, 761−766.
39. Bellanda, M., Peggion, E., Burgi, R., van Gunsteren, W., and Mammi, S. (2001) Conformational study of an Aib-rich peptide in DMSO by NMR, *J. Pept. Res. 57*, 97−106.
40. Venyaminov, S. Y., Hedstrom, J. F., and Prendergast, F. G. (2001) Analysis of the segmental stability of helical peptides by isotope-edited infrared spectroscopy, *Proteins 45*, 81−89.
41. Kise, K. J., Jr., and Bowler, B. E. (2002) Induction of helical structure in a heptapeptide with a metal cross-link: modification of the Lifson-Roig helix-coil theory to account for covalent cross-links, *Biochemistry 41*, 15826−15837.
42. Kemp, D. S., Boyd, J. G., and Muendel, C. C. (1991) The helical s constant for alanine in water derived from template-nucleated helices, *Nature 352*, 451−454.
43. Osapay, G., and Taylor, J. W. (1992) Multicyclic polypeptide model compounds. 2. Synthesis and conformational properties of a highly α-helical uncosapeptide constrained by three side-chain to side-chain lactam bridges, *J. Am. Chem. Soc. 114*, 6966−6973.
44. Qian, H., and Schellman, J. A. (1992) Helix-coil theories: A comparative study for finite length polypeptides, *J. Phys. Chem. 96*, 3987−3994.
45. Feldman, H. J., and Hogue, C. W. (2002) Probabilistic sampling of protein conformations: new hope for brute force? *Proteins 46*, 8−23.
46. Neves, D. E., and Scott, R. A., III (1976) Monte Carlo calculations on polypeptide chains. IX. A study of the effect of long-range interactions on the helix-coil transition, *Macromolecules 9*, 554−560.

BI048152K